Evaluation of imaging protocol for ECT based on CS image reconstruction algorithm*

ZHOU Xiao-Lin(周小林)[1,2,3] YUN Ming-Kai(贠明凯)[1,2] CAO Xue-Xiang(曹学香)[1,2]
LIU Shuang-Quan(刘双全)[1,2] WANG Lu(王璐)[1,2] HUANG Xian-Chao(黄先超)[1,2] WEI Long(魏龙)[1,2;1)]

[1] Key Laboratory of Nuclear Analytical Techniques, Institute of High Energy Physics, Chinese Academy of Sciences, Beijing 100049, China
[2] Beijing Engineering Research Center of Radiographic Techniques and Equipment, Beijing 100049, China
[3] University of Chinese Academy of Sciences, Beijing 100049, China

Abstract: Single-photon emission computerized tomography and positron emission tomography are essential medical imaging tools, for which the sampling angle number and scan time should be carefully chosen to give a good compromise between image quality and radiopharmaceutical dose. In this study, the image quality of different acquisition protocols was evaluated via varied angle number and count number per angle with Monte Carlo simulation data. It was shown that, when similar imaging counts were used, the factor of acquisition counts was more important than that of the sampling number in emission computerized tomography. To further reduce the activity requirement and the scan duration, an iterative image reconstruction algorithm for limited-view and low-dose tomography based on compressed sensing theory has been developed. The total variation regulation was added to the reconstruction process to improve the signal to noise Ratio and reduce artifacts caused by the limited angle sampling. Maximization of the maximum likelihood of the estimated image and the measured data and minimization of the total variation of the image are alternatively implemented. By using this advanced algorithm, the reconstruction process is able to achieve image quality matching or exceed that of normal scans with only half of the injection radiopharmaceutical dose.

Key words: ECT, imaging protocol, compressed sensing, total variation

PACS: 87.57.nf, 87.57.U-, 87.55.K- **DOI:** 10.1088/1674-1137/38/4/048201

1 Introduction

SPECT (Single-Photon Emission Computerized Tomography) and PET (Positron Emission Tomography) are established diagnostic tools that are widely appreciated in the clinical fields of oncology, neurology, cardiology and several others [1]. However, the lack of standardized acquisition protocols has been identified as a problem that limits their potential in lesion detectability and diagnosis confidence. Feasibility studies have previously been conducted [2–4] on optimizing the acquisition protocol between angle sampling and activity requirement, along with the extension of the use of these imaging tools. In general, the trade-off between image acquisition time and noise levels has been determined for the standard protocols and scan times. Images of better quality are obtained through larger numbers of samples and more acquisition counts, which means more radionuclide or longer acquisition time. However, in clinical settings, shorter acquisition times and lower radionuclide doses are preferable if the image quality is the same as that of a normal scan. Shorter acquisition times are beneficial for patients and allows higher throughput for screening applications [5]. Lower radionuclide doses reduce the risk of radiation exposure for patients and clinical staff [6].

Several studies have suggested the importance of optimizing acquisition times or the injected doses of radiopharmaceuticals to improve the quality of images in ECT (Emission Computerized Tomograph) [2, 7, 8]. However, these studies offered recommendations on acquisition protocol only by traditional reconstruction algorithms such as FBP (Filtered Back Projection) and MLEM (Maximum Likelihood Expectation Maximization). These algorithms deliver unsatisfactory and noisy results in those cases where acquisition time is shorter and radionuclide dose is lower. To tackle this challenge, the CS (Compressed Sensing) theory [9] has been introduced for image reconstruction. Moreover, several works

Received 28 June 2013, Revised 20 November 2013
∗ Supported by National Natural Science Foundation of China (81101175)
1) E-mail: weil@ihep.ac.cn

have used the a priori information of total variation to improve the quality of images in ECT reconstructions [10–12]. In this study, the CS based EM-TV (Expectation Maximization- Total Variation) algorithm is used to optimize the acquisition protocol. In the first part, the effect of sampling angle and counts per angle on the image quality is examined with both MLEM and EM-TV algorithms. The second part shows how the EM-TV algorithm can be used to halve both the acquisition time and the dose requirement while preserving image quality.

2 Methods and materials

Since the reconstruction algorithms have considerable effects on the acquisition protocol optimization, both traditional and CS-based reconstruction methods were evaluated, namely MLEM and EM-TV, respectively. Our study consists of two parts. In the first part, six sets of ECT simulation data with various angle numbers and counts per angle (with a fixed total imaging count) were acquired to evaluate how these two factors affect the image quality. The two reconstruction algorithms were used and the SNR (Signal to Noise Ratio) and CNR (Contrast-to-Noise Ratio) were calculated to evaluate the lesion detectability and diagnosis confidence. In the second part of the study, the EM-TV algorithm was prospectively used to develop the image protocol for half-acquisition. In other words, with the EM-TV algorithm, we expect to get the same or better image quality using a shorter acquisition time and fewer viewing angles than that of MLEM with full-acquisition.

2.1 Reconstruction algorithms

MLEM is a widely used iterative algorithm that maximizes the expectation maximization likelihood function [13]. The significant merit of this algorithm is that it can achieve much better image quality compared with that of FBP [14].

The formula for the MLEM algorithm is

$$f^{(k)}(i)=\frac{f^{(k-1)}(i)}{\sum p(i,j)}\sum\frac{p(i,j)d(j)}{\sum p(i',j)f^{(k-1)}(i')}, \qquad (1)$$

where $f^{(k)}(i)$ is the ith element of the reconstructed image at the kth iteration, $p(i,j)$ is the system matrix, which represents the probability of an event in pixel i being detected by LOR (Line Of Response) j, and $d(j)$ is the jth projection. The system matrix, which is a key factor in the MLEM algorithm, models the relationship between the reconstructed image and the projection data.

Common reconstruction algorithms, including MLEM, yield undesirable artifacts in reconstructed images with limited viewing angles and low dose data. The CS algorithm [9] is a well-established approach for signal recovery, which mainly relies on the sparsity recovery of the target signal. Based on the assumption that the target signal is of sparsity form, the power of the CS algorithm in dealing with the limited view and low dose cases has been acknowledged [15, 16]. The L1-minimized method is usually used to solve the constrained optimization problem in CS. The formula for the L1-minimized method is

$$\min\|\Psi f\|_1 \text{ s.t. } Mf=g, \qquad (2)$$

where Ψ is the sparsification transform, f is the true image, M is the system matrix and g is the measured data. The gradient transform is widely used as a sparsification transform in sparse-view image processing. Since medical images have sparsity in the gradient transform [17], it should be possible to reconstruct an accurate image by recovering the sparsity. Since the L1-norm of the gradient transform is the total variation, the expression of the L1-minimized method becomes

$$\min\|\Psi f\|_{\rm TV} \text{ s.t. } Mf=g. \qquad (3)$$

A two-step iterative method [18] is used to solve Eq. (3). The first step is to enforce measured data to the true activity where the traditional reconstruction methods can be applied. The next step is to minimize the TV of the image. This total variation based algorithm has been recently investigated in Cone-Beam Computed Tomography (CBCT) as the TV-POCS (Projection Onto Convex Sets) algorithm [19], which has been used to preserve edges, with the assumption that most images are piece-wise constant. However, the Poisson noise due to photon counting statistics in nuclear imaging may seriously disturb the TV-minimization. In this paper, the EM algorithm, which is considered to be superior under a Poisson noise distribution, was used in the first step, and the gradient descent method was used in the second step. The execution steps for this EM-TV algorithm are:

1) The EM-step:

$$f^k_{\rm EM}=\frac{f^{(k-1)}(i)}{\sum p(i,j)}\sum\frac{p(i,j)d(j)}{\sum p(i',j)f^{(k-1)}(i')}, \qquad (4)$$

2) The TV-step:

$$f^{k,l}_{\rm EMTV}=f^{k,l-1}_{\rm EMTV}+\alpha\frac{\overrightarrow{\nu}^{k,l-1}_{\rm TV}}{\left|\overrightarrow{\nu}^{k,l-1}_{\rm TV}\right|}, \qquad (5)$$

where

$$\overrightarrow{v}^{k,l-1}_{\rm TV}=\frac{\partial\|f\|_{\rm TV}}{\partial f}\Big|_{f=f^{k,l-1}_{\rm EMTV}}, \qquad (6)$$

and where k is the iteration number of the EM-TV method, l is the iteration number of the TV-step, and a is a relaxation factor to balance the two steps. $f^{k,0}_{\rm EMTV}$ in the TV-step should be set to $f^k_{\rm EM}$ in the EM-step and $f^{k-1}_{\rm EM}$ should be set to the output image of the TV-step in the last iteration. Since a could be related to the view numbers, we set different values for a in each experiment.

2.2 Simulation model

A single head SPECT with a low-energy, high-resolution collimator was simulated as a typical piece of ECT equipment by GATE (Geant4 Application for Tomographic Emission) [20]. The detector component of this equipment is composed of a 62×62 array of 2 mm×2 mm×6 mm NaI crystals. According to the energy resolution of the system, the energy window was set as a 20% symmetric window at 140 keV. To flexibly change the sampling angle, all of the scans were acquired with a circular orbit with uniform step-and-shoot acquisition over 360°. Six experiments were set with fixed total counts in the first part, as shown in Table 1. In the second part, half-acquisition data was selected for some view numbers, compared with the full-acquisition for the same angle numbers, as shown in Table 2. The scatter events have been rejected from the simulation data, as an accurate scatter correction before reconstruction.

Table 1. The six sets of experiments for the full-acquisition in Part 1.

Num. of sets	1	2	3	4	5	6
angle number	120	60	40	30	24	20
counts/angle ($\times 10^3$)	10	20	30	40	50	60
reconstruction algorithm	both MLEM and EM-TV					

Table 2. The six sets of experiments for comparison of half-acquisition and full-acquisition in Part 2.

	half-acquisition			full-acquisition		
Num. of sets	1	2	3	4	5	6
angle number	60	30	20	60	30	20
counts/angle ($\times 10^3$)	10	20	30	20	40	60
reconstruction algorithm	EM-TV			MLEM		

A cylinder phantom with internal diameter of 90 mm was simulated in this study. The activity concentration of ^{99m}Tc in the phantom background was 0.2 μCi/CC because this is a typical clinical activity concentration. Inside the phantom, six small cylinders with diameters of 18.5, 14, 11, 8.5, 6.5, and 5 mm were inserted and placed at a radial distance of 28.6 mm from the center of the phantom. The two largest cylinders (18.5 mm and 14 mm) were filled with water containing no radioactivity, for cold lesion imaging, whereas the four smaller cylinders (11 mm, 8.5 mm, 6.5 mm, and 5 mm) were filled with an activity concentration of 9:1 with respect to the background, for hot lesion imaging (Fig. 1).

2.3 Evaluation methods

A transverse image centered on the phantom was used for analysis and six circular ROIs (Regions of Interest) were drawn over the centers of the six inserted cylinders. Similarly, a circular ROI with a diameter of 30 mm was drawn on the center of the image as a background ROI.

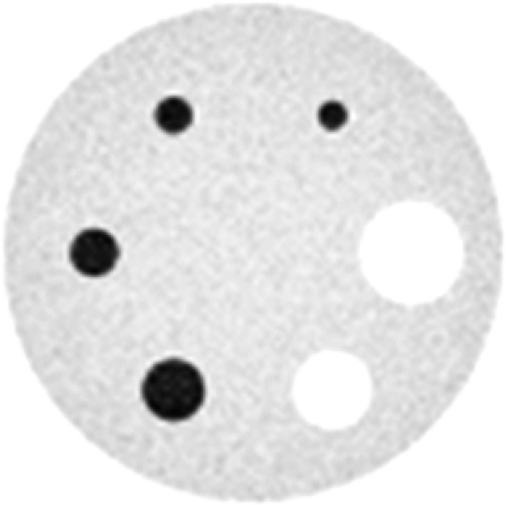

Fig. 1. Transverse image of the phantom.

To evaluate the detection rate of lesions and the evaluation accuracy, the SNR and CNR were used as a quality measurement.

$$SNR = \frac{M_{\rm bg}}{STD_{\rm bg}}, \tag{7}$$

$$CNR_{\rm hot} = \frac{M_{\rm hot}-M_{\rm bg}}{STD_{\rm bg}}, \tag{8}$$

$$CNR_{\rm cold} = \frac{M_{\rm bg}-M_{\rm cold}}{STD_{\rm bg}}, \tag{9}$$

where $M_{\rm hot}$ is the average of the hot ROI, $M_{\rm cold}$ is the average of the cold ROI, $M_{\rm bg}$ is the average of the background ROI, and $STD_{\rm bg}$ is the standard deviation of the background ROI. The comparison of SNR and CNR were plotted for each algorithm and each experiment under different iteration times.

3 Results

3.1 Part 1: Full-acquisition results

The six sets of simulated data (Table 1) were reconstructed by the MLEM algorithm and EM-TV algorithm with different iteration times. Although the sampling angles are fewer, it is apparent from Fig. 2 that the uniformity has been visibly increased for both MLEM and EM-TV results with more counts per angle.

The SNR and CNR curves for measurement of the lesion detectability are shown in Fig. 3. From the MLEM results, it can be seen clearly that a smaller view number can give higher SNR and CNR for a fixed total count after a certain number of iterations. The regularity was

about the same for the EM-TV results. Moreover, it is to be observed that: (1) the SNR and CNR of the EM-TV results were higher than that of MLEM results, (2) the SNR and CNR of the 30-view-angle experiment with EM-TV was a little distinctive, which was caused by the effect of Poisson noise in the TV-minimization step; however, there were signs that with an increase in number of iterations, which will eventually follow the regularity mentioned before.

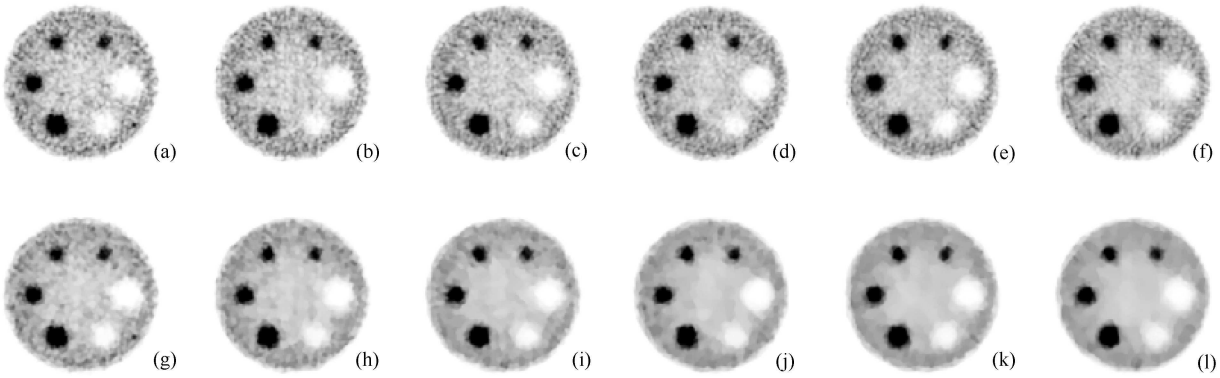

Fig. 2. The transverse images in the center slice after 30 iterations of full-acquisition using MLEM (top row) and EM-TV (bottom row), with the different view numbers and counts per angle given in Table 1. The total count is fixed and the (view numbers, counts/angle) of each experiment is (a, g) (120, 10×10^3); (b, h) (60, 20×10^3); (c, i) (40, 30×10^3); (d, j) (30, 40×10^3); (e, k) (24, 50×10^3); (f, l) (20, 60×10^3).

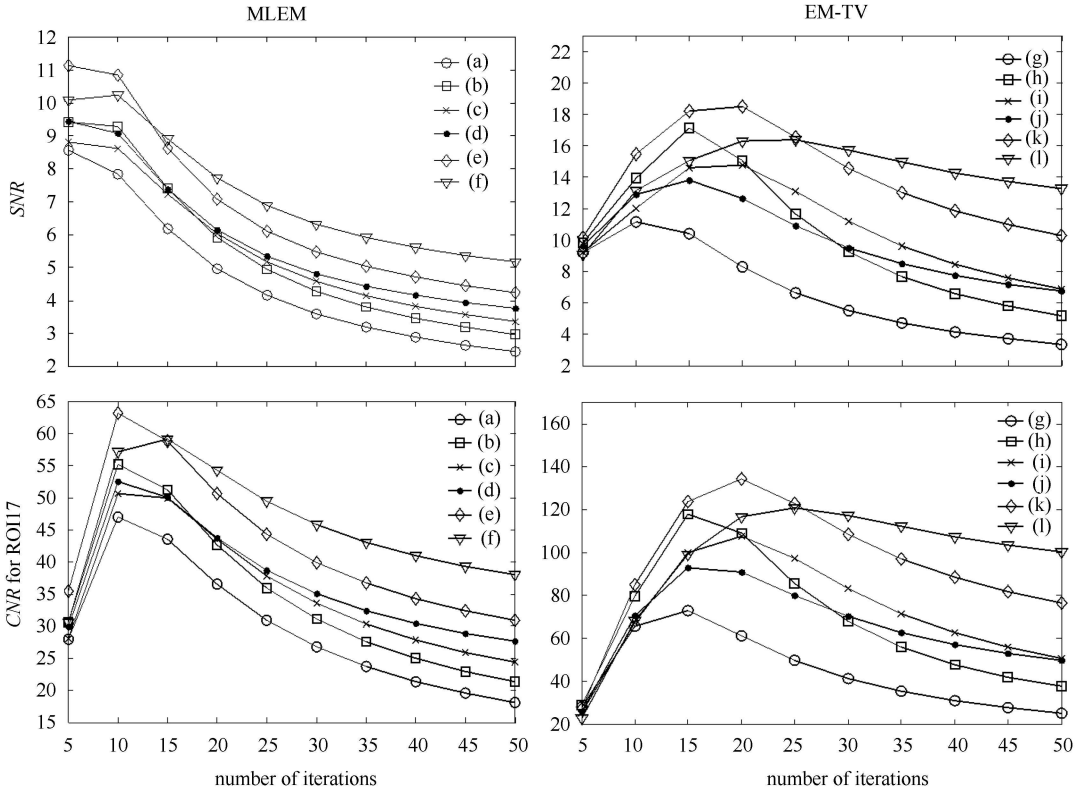

Fig. 3. The SNR and CNR of ROI17 vs. iteration times for the images in Fig. 2. The top row shows the SNR value, the bottom row shows the CNR value, the left column shows the MLEM results and the right column shows the EM-TV results.

3.2 Part 2: Half-acquisition results

To reduce the radiological dose and acquisition time, the images of comparative experiments in Table 2 are shown in Fig. 4. As expected, it is to be observed that, although the quality of (a) and (d) was about the same, the uniformity of (b) and (c) was much better than that of (e) and (f), respectively. Moreover, the artifacts were reduced effectively by the EM-TV method. The SNR and CNR vs. iteration times for the images in Fig. 4 are shown in Fig. 5. Compared with (a) and (d), the distinction of SNR or CNR was negligible. Meanwhile, the two metrics of (b) were obviously higher than that of (e). Furthermore, the improvement in (c) relative to (f) was the most significant in these three pairs of comparative experiments. That is, with half the counts/angle, EM-TV can give a greater advantage in the case of fewer view numbers.

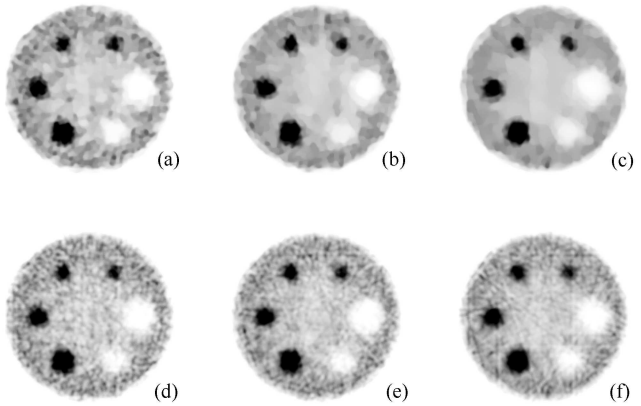

Fig. 4. The transverse images in the center slice after 30 iterations with half-acquisition using EM-TV (top row) and full-acquisition using MLEM (bottom row) in Table 2. The (view numbers, counts/angle) and reconstruction algorithm of each experiments is: (a) (60, 10×10^3)-EMTV, (b) (30, 20×10^3)-EMTV, (c) (20, 30×10^3)-EMTV, (d) (60, 20×10^3)-MLEM, (e) (30, 40×10^3)-MLEM, (f) (20, 60×10^3)-MLEM.

4 Discussion

In nuclear imaging, the radiation dose and imaging efficiency are of great concern. Therefore, in the first part of this study the sampling angle and the counts per angle were compromised so that better image quality could be obtained. The results of the experiments presented in Table 1 using both MLEM and EM-TV algorithms (Figs. 2, 3) revealed that the noise level per angle plays a more important role in the image quality. This will provide useful information for optimization of the measurement chain.

To reduce scan times and tracer requirements, noisier images are often allowed, which may result in inaccurate diagnosis, otherwise more γ detectors are introduced, which may increase the cost. The recently introduced iterative reconstruction algorithms, which incorporate noise regularization and resolution recovery, may provide a new alternative. In the second part of this study, a novel compressed sensing-based reconstruction algorithm was presented which uses significantly fewer measurements than traditionally required, thus demonstrating potential for reduction in scan time and radiopharmaceutical dose, with benefits for patients and health care economics. Several metrics, such as SNR and CNR, are used to compare the performance of the new method with traditional reconstruction algorithms. It is indicated by Fig. 4 and Fig. 5 that the new approach allows the same quality of images with 60 view angles, and higher quality images with 20 and 30 view angles. In other words, the image quality can be preserved or improved, even if the radiopharmaceutical injection dose and the scan time are reduced, which not only helps to reduce the harmful

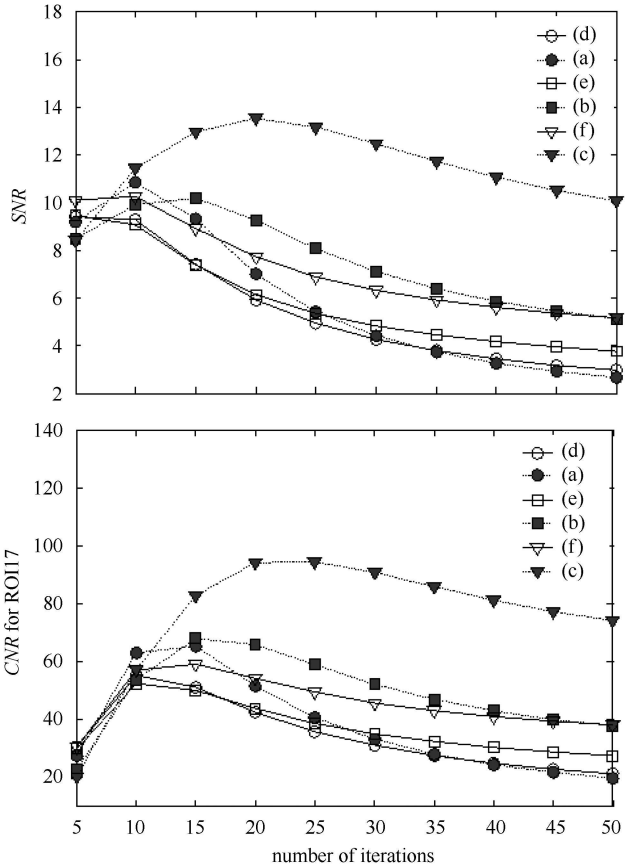

Fig. 5. The CNR of ROI17 vs. iteration times for the images in Fig. 4. The up figure shows the SNR value, the down figure shows the CNR value.

radiation dose to which patients and staff are exposed, but also enhances the scanning efficiency. The reduction of acquisition time should also lead to fewer motion artifacts, in accordance with greater scanning efficiency.

Another way to improve the performance of an imaging system is to incorporate the characteristic of the detector response in the reconstruction process as a resolution recovery algorithm. This work is in progress.

5 Conclusion

Under similar imaging counts, acquisition counts per angle should be considered to be more important than the sampling number in ECT. In addition, by using the CS-based EM-TV algorithm, the injected dose to the patient can be halved while obtaining even better, or at least the same, image quality compared with a full dose scan.

References

1 Green M, Seidel J, Vaquero J J et al. Computerized Medical Imaging and Graphics, 2001, **25**(2): 79
2 Takahashi Y, Murase K, Mochizuki T et al. Annals of Nuclear Medicine, 2003, **17**(7): 525
3 Masuda Y, Kondo C, Matsuo Y et al. Journal of Nuclear Medicine, 2009, **50**(6): 844
4 CHEN W P, Matsunari I, Noda A et al. Journal of Nuclear Medicine, 2005, **46**(10): 1633
5 Halpern B S, Dahlbom M, Quon A et al. Journal of Nuclear Medicine, 2004, **45**(5): 797
6 Ferretti A, Bellan E, Gava M et al. European Journal of Radiology, 2012, **81**(11): 3363
7 Vija A H, Zeintl J, Chapman J T et al. Development of Rapid SPECT Acquisition Protocol for Myocardial Perfusion Imaging. IEEE Nuclear Science Symposium Conference Record. 2006. 1811
8 Strauss L G, Pan L, Cheng C et al. Journal of Nuclear Medicine, 2011, **52**(3): 379
9 Donoho D L. IEEE Transactions on Information Theory, 2006, **52**(4): 1289
10 Sawatzky A, Brune C, Wubbeling F et al. Accurate EM-TV Algorithm in PET with Low SNR. Nuclear Science Symposium Conference Record. 2008. 5133
11 Muller J, Brune C, Sawatzky A et al. Reconstruction of Short Time PET Scans Using Bregman Iterations. Nuclear Science Symposium and Medical Imaging Conference. 2011. 2383
12 Wolf P, Sidky E, Schmidt T. A Compressed Sensing Algorithm for Sparse-View Pinhole Single Photon Emission Computed Tomography. Nuclear Science Symposium and Medical Imaging Conference (NSS/MIC) of 2011 IEEE, 2011. 2668
13 Shepp L A, Vardi Y. IEEE Transactions on Medical Imaging, 1982, **1**(2): 113
14 Chatziioannou A, QI J, Moore A et al. IEEE Transactions on Medical Imaging, 2000, **19**(5): 507
15 CHEN G H, TANG J, LENG S. Medical Physics, 2008, **35**: 660
16 Figueiredo M A, Nowak R D, Wright S J. IEEE Journal of Selected Topics in Signal Processing, 2007, **1**(4): 586
17 PAN X, Sidky E Y, Vannier M. Inverse Problems, 2009, **25**: 123009
18 Sidky E Y, PAN X. Physics in Medicine and Biology, 2008, **53**: 4777
19 Sidky E Y, Kao C M, PAN X. Journal of X-Ray Science and Technology, 2006, **14**(2): 119
20 http://opengatecollaboration.healthgrid.org/